THE JOURNAL OF PHYSICAL CHEMISTRY C

Article

pubs.acs.org/JPCC

Tuning Phosphorene Nanoribbon Electronic Structure through Edge Oxidization

Bangfu Ding,[†] Wei Chen,[‡] Zilong Tang,[§] and Junying Zhang*[,†]

[†]Key Laboratory of Micro-Nano Measurement, Manipulation and Physics (Ministry of Education), Department of Physics, Beihang University, Beijing 100191, China

[‡]Department of Physics, University of Texas at Arlington, Arlington, Texas 76019, United States

[§]State Key Laboratory of New Ceramics and Fine Processing, School of Materials Science and Engineering, Tsinghua University, Beijing 100084, China

Supporting Information

ABSTRACT: Molecular orbital theory predicts that interactions between lone-pair electrons give rise to van der Waals forces between layers due to the nonequivalent hybridization in bulk black phosphorus. First-principles calculations show that phosphorene nanoribbons (PNRs) have a high activity and can be bonded easily with oxygen atoms and hydroxyl groups, indicating that the PNRs can be oxidized easily. The cliff PNR configuration can be maintained when it is passivated with hydroxyl groups, indicating that it could be stable in a strong alkaline environment. Upon oxidation of their zigzag, armchair, and cliff edges, phosphorene nanoribbons can be changed from semimetallic to semiconducting, and the band gap can be changed from direct to indirect. OHO-[(OH + O)-] and OH- [(O + H)-] passivated PNRs have intrinsic spin magnetic moments of approximately 2.00 μ_B, which originate from the edge unsaturation electrons and the symmetry reduction. Therefore, oxidized PNRs might have potential applications in photoelectronic and spinelectronic devices.

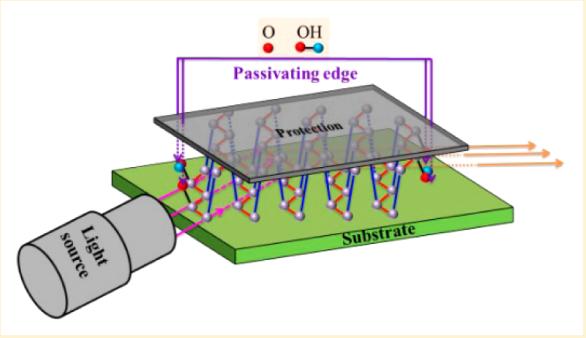

INTRODUCTION

Layered materials include graphite,[1] transition-metal dichalcogenides,[2] graphitic-phase carbon nitride (g-C_3N_4),[3] boron carbide (BC_3), boron nitride (BN), silicon (Si),[4] arsenic (As), and antimony (Sb).[5] The superior electrical and optical properties of graphene, such as ballistic transport and large coherence length, make it an excellent platform for studying quantum electrodynamics phenomena.[6] Many studies of the electronic, mechanical, optical, thermal, and magnetic properties of graphene have been published. However, the zero band gaps of graphene, silicene, and germanene represet a major weakness that restricts their applications. Various methods have been employed to tune their electronic structures, and new layer materials are also being explored. Changing the number of layers and the packing mode[7] can easily tune the band gaps of such materials. Moreover, cutting layered materials into lower-dimensional forms such as one-dimensional nanoribbons, nanowires, nanorods, and nanotubes or zero-dimensional quantum dots can also open their zero band gaps to finite values. For example, graphene quantum dots have color-tunable photoluminescence, ranging from the visible to the near-infrared regions as a result of quantum size or edge state effects.[8] Hence, they are promising candidates for applications in carbon-based electronic and magneto-electronic devices, as well as light-emission diodes.[9]

Bulk black phosphorus consists of puckered two-dimensional honeycomb stacking layers. Upon the exfoliation of bulk black P, mono- and few-layer black P materials (called as phosphorene) have successfully been obtained.[10] These are novel two-dimensional direct-band-gap semiconductors. For bulk materials, the fundamental band gap is 0.30 eV, and for a single layer, the band gap is 2.0 eV.[11] According to experimental and theoretical studies, phosphorene displays interesting electrical, magnetic, and optical properties. Single-layer phosphorene has an extremely high hole mobility on the order of 10000 $cm^2\ V^{-1}s^{-1}$ and anomalous elastic properties with anisotropy.[12] Its optical absorption spectrum indicates linear dichroism between perpendicular in-plane directions. Thus, it is possible to use optical measurements to determine the crystal orientation and to activate the anisotropic transport properties by light.[12] In addition to light absorption spectra, Raman spectra have been shown to be very useful for the determination of crystalline orientation.[13,14] For a bilayer, different stacking orders can adjust the band gaps from 0.78 to 1.04 eV.[15] Few-layer phosphorene shows a robust direct-band-gap character, and its band gap decreases with the number of layers following a power law.[16] Aside from the intrinsic tunable

Received: September 19, 2015
Revised: December 28, 2015
Published: January 5, 2016

DOI: 10.1021/acs.jpcc.5b09159
J. Phys. Chem. C 2016, 120, 2149−2158

properties and methods to tune the band gap, effective mass and transport properties have also been investigated. The phosphorene band gap decreases with increasing compressive strain, and a semiconductor-to-metal transition appears upon the application of a biaxial compressive strain. In contrast, tensile strain can enlarge the band gap.[17] Electric fields also have an influence on phosphorene similar to that of strain.[17] Many theoretical and experimental methods have been applied to explore potential properties or achieve new morphologies of phosphorene.[18−20]

From first-principles calculations, it is known that one-dimensional zigzag graphene nanoribbons are half-metallic. However, armchair graphene nanoribbons are semiconductors, as discussed in the literature.[6,21] Similarly, one-dimensional phosphorene such as nanoribbons or nanotubes might also have many superior properties according to theoretical predictions.[22] Although phosphorene nanoribbons (PNRs) have not yet been fabricated, they will likely be prepared in the future, because phosphorene quantum dots have been synthesized successfully.[23] Theoretical predictions of the electronic structures and optical responses of PNRs are essential for future applications of phosphorene-based optoelectronic devices. According to the cutting direction, PNRs contain different edges such as armchair, zigzag, and diagonal.[24] Their band gaps are highly dependent on the ribbon width, orientation, and strength of strain.[25] Under the effect of strain, these three structures with hydrogen passivation show different quantum size effects according to density functional theory (DFT). For instance, strain can effectively tune the charge-carrier transport properties, leading to a sudden increase in electron or hole effective mass and a transition from a direct band gap to an indirect band gap.[24] Because of the presence of edge states, the edges can adsorb foreign atoms for bonding to achieve a stable structure or reconstruct to enlarge the unit cell.[26] Therefore, different edge functionalization ions or groups such as hydrogen, fluorine, chlorine, oxygen, sulfur, selenium, and hydroxyl groups have been investigated for a series of ribbon widths up to 3.5 nm.[27] Adjusting the edge passivation was found to be a good approach to tuning the electronic structure. However, two critical problems arise. One is how the PNR structure changes after adsorbing two or more impurities at edges. The other is determining which configuration is relatively more stable when edge-passivated with single or mixed elements (groups).[28]

When black P is exposed to an oxygen environment, it is easily oxidized.[29] Similarly, PNRs have the same problem in the ambient atmosphere. Thus, it is necessary to study the influence of oxygen on the structure and the stability of PNRs. In this work, using first-principles calculations, we investigate the geometrical configurations and stabilities of PNRs that have been edge-passivated with hydrogen, hydroxyl groups, and oxygen, as well as their mixtures. The arrangement and bonding directions of the impurity atoms with the edge P atoms are dependent on the structures of the PNRs and the properties of the impurities themselves. Through an analysis of the optimized lattices and formation energies, we investigated the influence of these impurity atoms on the geometric structures, reactivities, and relative stabilities of PNRs. On the basis of molecular dynamics (MD) simulations, we also measured the room-temperature stabilities. From the theoretical predictions in this work, PNR exciton luminescence covering the visible and near-infrared regions is anticipated through edge oxidization using different species. Oxidized zigzag and armchair PNRs also have considerable spin magnetic moments, possibly due to unpaired electrons and the absence of an inversion center. This study can instruct some experiments on selectively oxidizing PNRs by adjusting the environmental conditions, with the purpose of tuning their photoelectronic or spinelectronic properties.

MODEL AND CALCULATION METHODS

Electronic structure calculations were performed by applying the projector-augmented wave pseudopotential method within the DFT framework.[30] All calculations were completed using the Vienna Ab Initio Simulation Package (VASP).[31] The constituted atomic valence states were treated as O ($2s^2$, $2p^4$), P ($3s^2$, $3p^3$), and H ($1s^1$). The other electronic states were frozen as core states. The kinetic energy cutoff for the plane-wave basis set was determined to be 500 eV. The energy and Hellmann−Feynman force convergence criteria for electronic and ionic iterations were set at 1×10^{-4} eV and 0.01 eV/Å, respectively. The geometry optimization was carried out with the Perdew−Burke−Ernzerhof (PBE) functional. Self-consistent electronic structure calculations were performed with the PBE and the Heyd−Scuseria−Ernzerhof (HSE06) hybrid functionals. For the zigzag, armchair, and cliff PNR structures shown in Figure 1, the reciprocal spaces were meshed at $3 \times 1 \times 1$, $1 \times 1 \times 3$, and $4 \times 1 \times 1$ using Monkhorst−Pack meshes centered at the Γ point in all calculations. A vacuum of at least 12 Å was included in the supercell to avoid spurious interactions. All calculations contained spin polarization. According to previous calculations,[32,33] van der Waals force corrections such as the Grimme, Becke−Jonson, and Tkatchenko−Scheffler methods are dispensable to include in all simulations of phosphorene and PNRs. Hydrogen, hydroxyl, and oxygen passivation on the phosphorene edges or adsorption at the surfaces are not physical but chemical processes involving the formation of bonds with phosphorus atoms. To study the stability of the oxidized PNR structure at room temperature (300 K), we performed MD simulations for relatively stable configurations. Moreover, the room-temperature stabilities of HH-passivated PNR configurations were also checked by MD simulations. The models and electronic and spin densities were plotted with the Visualization for Electronic and Structural Analysis (VESTA) program.[34]

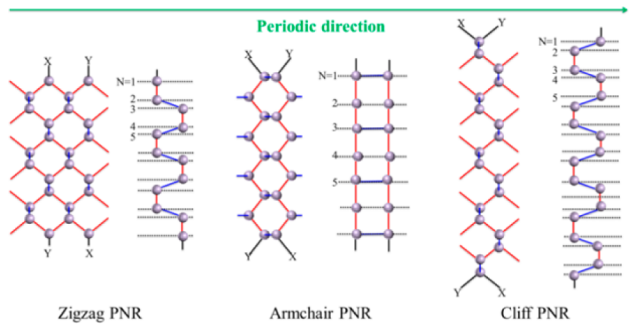

Figure 1. Top and side profiles of zigzag, armchair, and cliff PNRs. X and Y denote free atoms such as oxygen and hydrogen or groups such as hydroxyl. The horizontal green solid arrow and black dashed lines represent the periodic direction and dimer lines, respectively.

RESULTS AND DISCUSSION

PNR Structures and Edge Activities. There are a large number of stable phosphorus structures, such as white (having

DOI: 10.1021/acs.jpcc.5b09159
J. Phys. Chem. C 2016, 120, 2149−2158

α and β phases), red, violet, blue, and black allotropes. Moreover, theoretical predictions also propose the possible existence of stable γ-, ε-, η-, θ-, and δ-phosphorus.[35,36] Bulk black phosphorus, with space group *Cmca* (No. 64, D_{2h}^{18}), is the most stable form. The initial structure of phosphorene can be peeled off from the bulk counterpart[37,38] with a spatial symmetry of D_{2h}^{7} (*Pmna*, No. 53). The experimental bulk lattice parameters are a = 3.3136 Å, b = 10.4780 Å, and c = 4.3736 Å with $\alpha = \beta = \gamma = 90°$. In phosphorene, each P atom is coordinated by three adjacent P atoms with bond lengths of 2.24 and 2.22 Å, as shown in blue and red in Figure 2a. Because the outermost shell of each P atom has five electrons with a $3s^2 3p^3$ configuration, the P atoms form sp^3 hybridization to constitute three bonds according to hybridization orbital theory. The remaining two electrons form a lone pair. Thus, the hybridization is nonequivalent, and the bond angles are not 109.47° but 96.34° for ∠AOB and 102.09° for ∠AOC and ∠BOC. The lone-pair electrons can easily bond with foreign impurities such as oxygen and nitrogen.[39−41] That is, oxygen or nitrogen can saturate the lone-pair electrons to convert nonequivalent sp^3 hybridization to normal sp^3 hybridization. Schematics of the hybridization process and bonding structure are displayed in Figure 2b. Moreover, the van der Waals forces make layer-to-layer linkages through the Coulomb interactions of lone-pair electrons, as shown in Figure 2c.

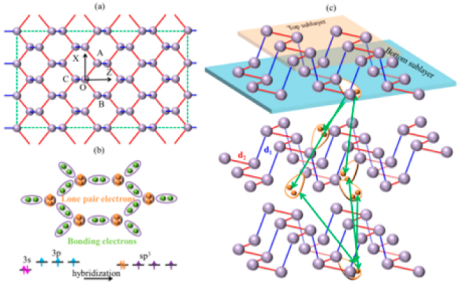

Figure 2. Schematics of (a) the structure of phosphorene, (b) the bonding structure and sp^3 hybridization process, and (c) the mechanism of van der Waals force formation between adjacent layers. The small yellow and green balls represent the lone pairs and bonding electrons, respectively. The separation distance between neighboring layers is approximately 5.0−5.5 Å.

Three classes of phosphorene structures denoted as zigzag, armchair, and cliff-like plane configurations have been established. The original and optimized configurations of these structures are shown in Figure S1. These three architectures have two-dimensional periodicity along the X and Z axes. The optimized lattice parameters and energies per P atom are reported in Table S1. The lattice parameters are slightly different from the previous experimental values.[37,38] The single P-atom energies in these three super cells are almost equal. Actually, these three structures are infinitely large planar configurations because of their periodic arrangements, and thus, all of the properties and crystal parameters are identical. For example, the band gaps, bond lengths, and bonding modes are almost equal, as shown in Table S1 and Figure S2. PBE and HSE calculations predict indirect and direct band gaps,

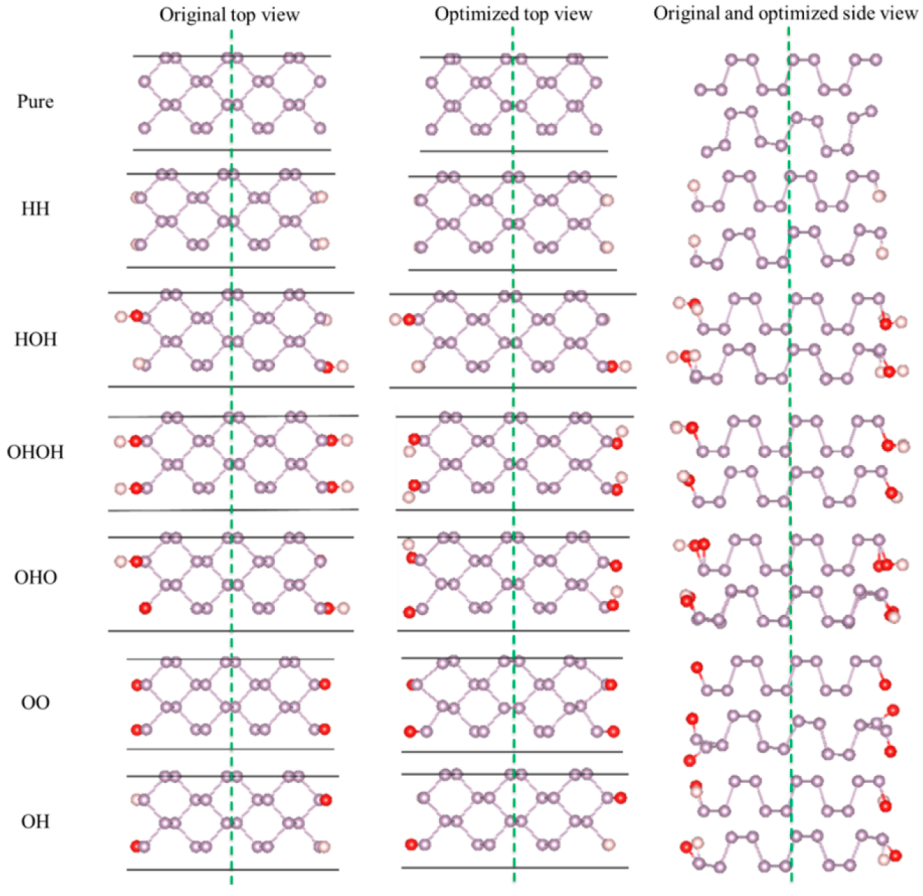

Figure 3. Original and optimized configurations of zigzag PNRs without and with edge passivation viewed from the top and side directions.

DOI: 10.1021/acs.jpcc.5b09159
J. Phys. Chem. C 2016, 120, 2149−2158

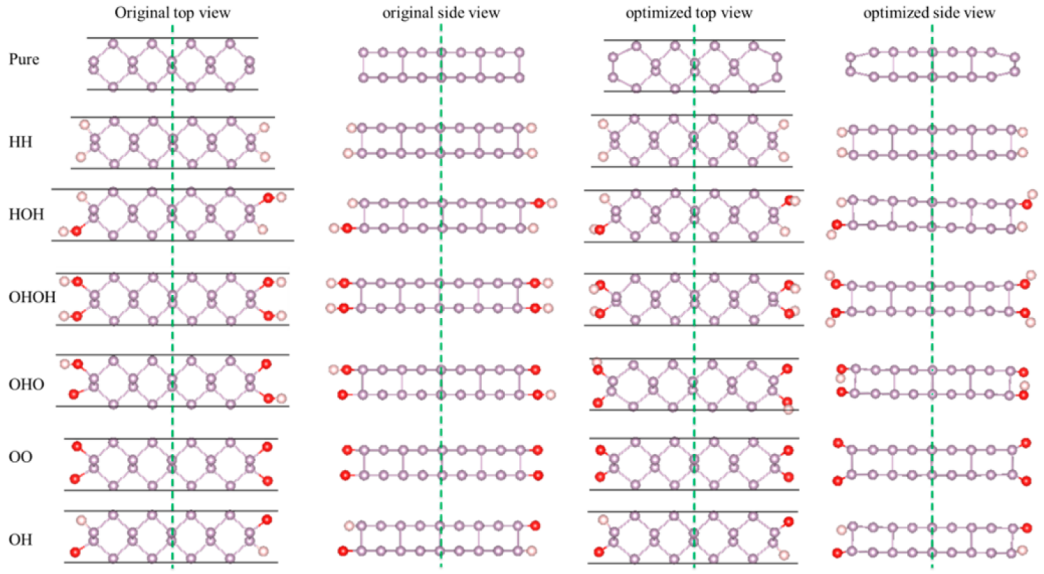

Figure 4. Original and optimized configurations of armchair PNRs without and with edge passivation viewed from the top and side directions.

respectively, for phosphorene. The HSE-calculated band-gap values are consistent with the previous GW-BSE calculation value 1.40 eV, as well as the experimental value of 1.45 eV from the photoluminescence spectrum.[42,43] Therefore, we mainly consider the HSE calculation results for electronic properties in this work. The relaxed crystal structures were optimized using the PBE functional; thus, the formation energies were computed with the PBE functional.

Slicing along the *X* direction, the PNRs have two types of edge configurations, namely, zigzag and cliff edges.[44] Similarly, armchair PNRs can be formed by cutting along the *Z* axis. For PNRs, the edges exhibit high activities because of the presence of one or two dangling bonds and easily absorb foreign impurities to achieve saturation, form deformations, or even reconstruct at the edges with a subsequent doubling of the unit cell along the periodic direction.[44] According to the experiment results, few-layer phosphorene samples are oxidized easily under ambient atmosphere.[45] Therefore, we investigate three PNR structures, exploring the influence of edge passivation using different species, including hydrogen, oxygen, and hydroxyl groups, on the activity, stability, electronic, and spin properties. These free radicals and groups were placed symmetrically on both sides of the PNRs, as displayed in Figure 1. For convenience, the edge-saturated structures are expressed as XY-passivated (terminated or saturated) PNRs with X (Y) = hydrogen, oxygen, and hydroxyl.

Zigzag PNRs. Top and side views of the original and optimized configurations are displayed in Figure 3. If the dimer line number N is $2n$ (n = 1, 3, 5, ...), then zigzag PNRs are nonsymmetric and symmetric when viewed from the top and side, respectively. When N is $2n$ with n = 2, 4, 6, ..., the results are just the opposite, as shown in Table S2. We take the latter case for calculation because odd and even numbers in zigzag PNRs are equivalent. Table S2 also lists the relationship between the dimer line number and the symmetry for armchair and cliff PNRs. In comparison with the original PNRs, all atom positions, bond lengths, and directions in the relaxed PNRs vary to different degrees. The variations in bond lengths (d_2) at the boundary are larger than those in the interior. From the side profiles, the P atoms at the two sides of the ribbon move in opposite directions. For the edge-passivated PNRs, all of the atomic positions and bond lengths change very little during the relaxation from the initial structures. Thus, the boundary P atoms in the XY-passivated PNRs return to the nonequivalent sp^3 hybridization. The edge passivation helps maintain the overall lattice frame of PNRs.

In the HH-, HOH-, and OH-passivated zigzag PNRs, the individual hydrogen atoms are always oppositely bonded with the edge P atoms on the two sides. In the OHO-terminated zigzag PNRs, the oxygen and the hydroxyl group tend to move closer to the center as a result of the bonding of solo oxygen and hydrogen in the hydroxyl group. Moreover, the OHO-termination effect induces the doubling of single cells and the disappearance of an inversion center. In the OO-saturated case, the two oxygen atoms move in opposite directions. One O—P bond is invariably perpendicular to the phosphorene plane, and the other O—P bond makes a 38° angle with the phosphorene plane. In the HOH-passivated PNRs, the direction of the hydroxyl bonds is parallel to that of the nanoribbon width, namely, armchair orientation. These bond directions in OHOH- and OHO-passivated PNRs are parallel to the zigzag or periodic direction. In summary, the edge P atoms show different activities for adsorbing foreign atoms to form oxidized or hydrogenated PNRs. The deformation or distortion degree of the bonds between edge P atoms and the adjacent P atoms in PNRs passivated by H-containing species are stronger than those in PNRs passivated by other species. This might indicate that PNRs are easy to oxidize, but not to hydrogenate; that is, oxygen- and hydroxyl-edge-saturated PNRs are more stable.

Armchair PNRs. In the same way, the original configurations and the final optimized constructions are displayed in Figure 4. In the optimized pristine structure, the internal P-atom positions and their bond lengths are similar to those in the original configuration. Because of the dangling bond of the P atoms on both sides, after geometry optimization, the edge P atoms move toward the nanoribbon center, and the bond length (d_1) changes from 2.24 to2.11 Å. A possible reason is the distortion/deformation effect.[46] Under oxidization and hydrogenation conditions, the edge P-atom positions change a little bit, and the P—P bond lengths vary slightly from 2.24 to 2.25 Å (2.25 Å on the other side), 2.23 (2.24), 2.23 (2.23), 2.32 (2.32), 2.25 (2.25), and 2.28 (2.30) Å for the HH-, HOH-,

DOI: 10.1021/acs.jpcc.5b09159
J. Phys. Chem. C 2016, 120, 2149−2158

OHOH-, OHO-, OO-, and OH-passivated configurations, respectively.

The variations in the individual hydrogen and oxygen atoms are identical in all structures; for example, the H—P and O—P bonds are located in the phosphorene plane. The only difference is that the O—P bonds are longer than the H—P bonds. The P—O (single oxygen) bond lengths in the OHO-, OO-, and OH-passivated PNRs are 1.54, 1.49, and 1.51 Å, respectively. Moreover, the hydrogen atom in OHO-passivated PNRs prefers to move to the single O atom to form a hydrogen−oxygen bond, and this H—O bond length was calculated as 1.49 Å after optimization. In the HOH-, OHOH-, and OHO-passivated PNRs, the hydroxyl group behaviors were similar. For example, the angles between the hydroxyl bond and the phosphorene plane were calculated to be 108°, 107°, and 117°, respectively, for these three structures. Considering the results for both the armchair and zigzag PNRs, it is concluded that the adsorption of impurities can stabilize the PNR edges, thus reducing the activity of the edge P atoms .

Cliff PNRs. Figure S3 displays the original and optimized configurations of pure and XY-passivated cliff PNRs. For the initial and relaxed pristine PNRs, the edge P atoms on both sides show substantial distortions and deformations, bonding to the neighboring P atom to recover the nonequivalent sp^3 hybridization. The P—P bond length decreases slightly from 2.24 to2.23 Å in reconstruction, rather than making the unit cell expand to double the original size according to Peierls theory.[46] The four edge P atoms on two sides of the relaxed configuration constitute barriers for the internal P atoms. As a result, the inner P-atom positions are hardly changed during the relaxation process. Obviously, the independent hydrogen-atom arrangements in HH-, HOH-, and OH-passivated PNRs are completely different from those in zigzag and armchair PNRs. In HH-passivated PNRs, the angle between two P—H bonds is almost 90°. One is parallel to the cliff phosphorene plane, whereas the other is perpendicular to the plane (Figure S3). In HOH-passivated PNRs, the P—H (single H) bonds are almost parallel to the cliff edge. However, the P—H bonds in OH-passivated PNRs disappear, and new P—O—H double bonds are formed. That is, hydrogen bonds with oxygen instead of P form.

The adsorption behaviors of oxygen atoms in OHO-, OO-, and OH-passivated PNRs are complicated during the relaxation process. For example, in OHO-passivated PNRs, the oxygen atoms on one side form two P—O bonds and one O—H bond, whereas those on the other side constitute a single P—O—O—H bond. These results indicate that the two sides of PNRs have different activities toward oxygen and hydroxyl species. Furthermore, the hydroxyl groups on the two sides of HOH- and OHOH-passivated PNRs show different arrangements. For example, after optimization from the original configuration in HOH-passivated PNRs, the P—O—H double bonds are retained, whereas the H—O bond direction rotates clockwise. In OHOH-passivated PNRs, the hydroxyl groups are unable to be adsorbed to the PNR edges, but transfer two hydroxyl groups to two individual H_2O_2 molecules, meanwhile recovering the PNR configuration to the unpassivated one. However, after being edge-treated using hydroxyl groups, cliff PNRs improve in stability, as discussed below.

Zigzag, armchair, and cliff PNRs show different adsorption capacities for XY free ions or groups to achieve stable structures. In these three edge-unpassivated PNRs, the edge P atoms reach stable states through large deformations or reconstructions. Thus, the bond lengths and directions change during the relaxation process to maintain equilibrium states. Through XY passivation, the edge P atoms reach sp^3 hybridization. X and Y show different adsorption behaviors on the edge of the PNRs. The symmetries of all of the pure PNRs are $P2/m$ (C_{2h}^1) with an inversion center, as shown in Table 1. In addition, some new spatial structures such as $P2_1/m$ (C_{2h}^2), $P\bar{1}$ (C_1^1), $P2_1$ (C_2^2), and Pm (C_s^1) appear in XY-terminated PNRs. The space symmetries $P\bar{1}$, $P2_1$, and Pm have no inversion center, causing spin splitting and moments. The symmetry changes originated from the edge states and the reconstruction of the adsorbed atoms. Therefore, edge passivation can induce new electronic properties, as discussed further below.

Table 1. Space Groups of Geometrically Optimized Zigzag, Armchair, and Cliff PNRs without and with Edge Passivation

passivation	zigzag	armchair	cliff
none	$P2/m$ (C_{2h}^1)	$P2/m$ (C_{2h}^1)	$P2/m$ (C_{2h}^1)
HH	$P2/m$ (C_{2h}^1)	$P2/m$ (C_{2h}^1)	$P\bar{1}$ (C_1^1)
HOH	$P2_1/m$ (C_{2h}^2)	$P\bar{1}$ (C_1^1)	$P\bar{1}$ (C_1^1)
OHOH	$P\bar{1}$ (C_1^1)	Pm (C_s^1)	$P\bar{1}$ (C_1^1)
OHO	$P2_1$ (C_2^2)	$P\bar{1}$ (C_1^1)	$P\bar{1}$ (C_1^1)
OO	$P2/m$ (C_{2h}^1)	$P2/m$ (C_{2h}^1)	$P\bar{1}$ (C_1^1)
OH	$P2_1/m$ (C_{2h}^2)	$P\bar{1}$ (C_1^1)	$P\bar{1}$ (C_1^1)

Relative Stability of PNRs. For XY-terminated PNRs, it is important to investigate their relative stabilities to understand which atoms or groups can be chemically or physically adsorbed on the edges. For pure and oxidized or hydrogenated PNRs, we applied the formation energy to evaluate their stability.[47,48] The formation energy is defined as the energy needed by the compounds to release or adsorb foreign elements and is expressed as

$$E_{\text{formation}} = E_{\text{PNRs}}\,(\text{pure or passivated}) - n_{\text{P}}\mu_{\text{P}} - \sum_{i=\text{H,O,or O+H}} n_i\mu_i \quad (1)$$

where E_{PNRs} is the total energy of pure or edge-passivated PNRs; n_i is the number of the ith impurity on the PNRs; μ_{P} is the energy per atom of a phosphorene sheet, as listed in Table S1; and μ_{O} and μ_{H} are calculated as $\mu_{\text{O}} = (E_{\text{O}_2}/2)$ and $\mu_{\text{H}} = (E_{\text{H}_2}/2)$ with molecular energies E_{O_2} for oxygen and E_{H_2} for hydrogen, as listed in Table S3. Here, we consider only H- and O-rich environments, but not P-rich environments.[48] From eq 1, the formation energies for the three types of PNRs are plotted in Figure 5.

The formation energies ($E_{\text{formation}}$) for the three classes of PNRs are basically similar according to computations using the PBE functional. For the three pure PNRs, the $E_{\text{formation}}$ values are positive, indicating that the two bare sides have high activities and can easily absorb foreign atoms or distort/reconstruct to reach energy minima. For all of the edge-passivated zigzag, armchair, and cliff PNRs, the $E_{\text{formation}}$ values are negative (except for HH-passivated cliff PNRs), indicating increased stability. The $E_{\text{formation}}$ values for zigzag and armchair PNRs edge-passivated by species containing oxygen or hydroxyl groups are smaller than those for such PNRs passivated by HH. Thus, the PNRs are easier to oxidize than to hydrogenate. The formation energy of OHOH-passivated cliff PNRs is slightly

DOI: 10.1021/acs.jpcc.5b09159
J. Phys. Chem. C 2016, 120, 2149−2158

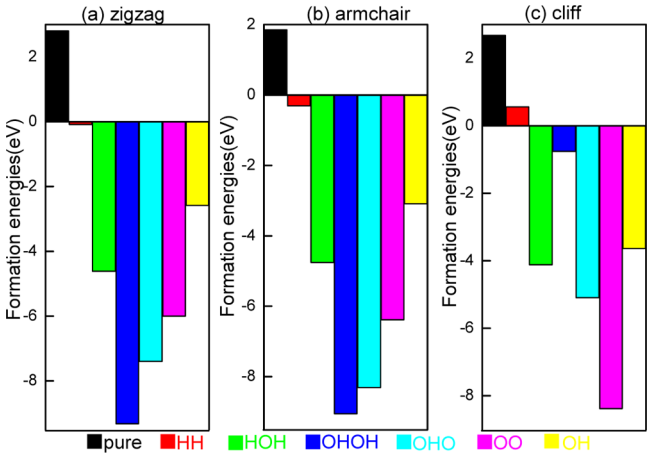

Figure 5. Formation energies of (a) zigzag, (b) armchair, and (c) cliff PNRs without and with XY passivation according to PBE functional calculations.

less than zero, which is attributed to the formation of hydrogen peroxide molecules, as mentioned above (Figure S3).

In addition, the formation of hydrogen bonds can increase the stability. For example, OHOH-passivated zigzag and armchair PNRs have the strongest stability, possibly because of the formation of hydrogen bonds. This has been verified for graphene nanoribbons,[49] where the stability of the zigzag configuration can be enhanced by OHOH passivation, and the main reason has been attributed to hydrogen bonding between adjacent hydroxyl groups. There are also hydrogen bonds in OHO-terminated zigzag and armchair PNRs, which have slightly lower stabilities than OHOH-passivated zigzag and armchair PNRs but higher stabilities than the other configurations. Therefore, different hydrogen-bonding chains might give different stabilities. The trends in $E_{formation}$ variations are similar to those of the Gibbs free energy for zigzag graphene nanoribbons with hydrogen I, hydrogen II, lactone, ketone, ether I, and ether II symmetry-edge terminations.[49] A comparison of $E_{formation}$ values for the three PNRs suggests that the PNR edges are anisotropic[50] and that the saturation or distortion/reconstruction of the edge states can increase PNR stability.

In addition to the two sides, the internal P atom can adsorb the foreign impurities to achieve normal sp^3 hybridization. The upper and lower surfaces of graphene can attract foreign atoms such as hydrogen and oxygen.[51] The two sides and surfaces compete to adsorb impurities. Therefore, the adsorptions of hydrogen, oxygen, and hydroxyl group on the phosphorene surfaces need to be examined. A 2 × 3 super cell of a zigzag-like phosphorene sheet containing 24 P atoms was built as shown in Figure S1a. These three ions and groups were placed on the sheet arbitrarily. The original and optimized structures are displayed in Figure S4. The optimized P—H, P—O, P—O, and O—H bond lengths were found to be 1.49, 1.51, 1.48, and 0.98 Å, respectively. For phosphorene adsorbing a single hydrogen, the P—H bond was almost perpendicular to the sheet. For phosphorene adsorbing oxygen and hydroxyl group, the angles between the P═O bond and phosphorene plane were 48.11° and 99.99°, respectively. Such behaviors are similar to those of small molecules such as CO, CO_2, NH_3, NO, and NO_2 adsorbed on phosphorene.[52]

The formation energies for hydrogen, hydroxyl, and oxygen to adsorb on the P sheet as calculated according to eq 1 are reported in Table 2. Comparison of the formation energies of PNRs edge-passivated and phosphorene surface-adsorbed by

Table 2. Formation Energies of Adsorbing Hydrogen, Oxygen, and Hydroxyl on the Surface of Phosphorene According to PBE Functional Calculations

adsorbing species	$E_{formation}$ (eV)
hydrogen	1.0390
oxygen	−1.8912
hydroxyl	−1.3901

the same species indicates that hydrogen and hydroxyl groups are easier to bond to the edge P atoms than to the phosphorene surface in zigzag and armchair PNRs, whereas the adsorption and passivation processes compete with each other in the cliff configuration. The oxygen atoms are prone to bond with edge rather than internal P atoms for all three types of PNRs. When the PNRs are edge-passivated using atom groups composed of both oxygen and hydrogen, the formation energies become smaller than those for only oxygen or hydrogen atoms. In general, free ions or groups are prone to bond with unsaturated edge P atoms. Moreover, in special cases, they can also be adsorbed by the lone-pair electrons of surface P atoms.

From the results of the first-principles calculations in this work, the formation energies for OO-edge-passivated PNRs were found to be much smaller than those of oxygen-surface-adsorbed PNRs. This means that oxygen atoms are preferentially adsorbed to edge P atoms to saturate the dangling bonds and then to middle P atoms on the surfaces. Therefore, the dissociation of oxygen molecules on the phosphorene surface is inevitable. To avoid surface oxidization, several works reported that the surfaces of phosphorene can be protected by more stable two-dimensional materials, such as graphene,[53] hexagonal BN,[54] and coating with a protective layer such as Al_2O_3[55,56] and SiO_2.[57] Finally, the two-dimensional Brillouin zones, energy bands, and electronic densities for hydrogen, hydroxyl group, and oxygen adsorbing on phosphorene sheet are displayed in Figures S5−S8. The hydrogen and hydroxyl adsorptions introduce two midgap states due to dangling bonds, whereas O adsorption does not cause any local states.

In the above discussion, we used the formation energy to evaluate the stability of oxidized PNRs at 0 K. Here, a molecular dynamics simulation at 300 K is applied to HH- and OHOH-passivated zigzag PNRs, HH- and OHOH-passivated armchair PNRs, and HH- and OO-passivated PNRs. As shown in Figure 6, the total energies fluctuated in a small range, indicating that edge-oxidized PNRs can be stable at room temperature. For the same configuration, the total energies of PNRs terminated with oxygen and hydroxyl group are lower than those of PNRs passivated by hydrogen. Thus, the edges prefer to adsorb oxygen and hydroxyl groups at 300 K, similarly to the case at 0 K.

Electronic and Spin Properties of PNRs. The energy bands, densities of states, and band gaps of PNRs have been reported.[58−60] The band gaps are strongly dependent on internal factors such as ribbon width and external factors such as electric field and strain.[58−60] The band gaps of PNRs can also be tuned by adjusting the edge-passivation groups such as hydrogen, fluoride, hydroxyl, oxygen, sulfur, and selenium.[27] However, the electronic structures of PNRs that have been edge-passivated by atom groups containing both oxygen and

DOI: 10.1021/acs.jpcc.5b09159
J. Phys. Chem. C 2016, 120, 2149−2158

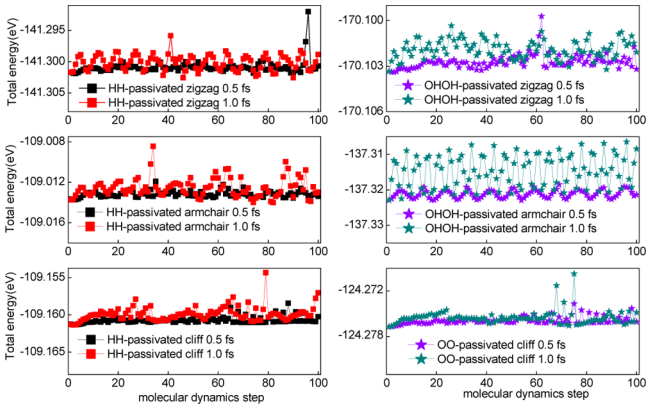

Figure 6. Changes in total energy with ion step in time steps of 0.5 and 1.0 fs for HH- and OHOH-passivated zigzag PNRs, HH- and OHOH-passivated armchair PNRs, and HH- and OO-passivated cliff PNRs.

hydrogen have not yet been reported, particularly for cliff nanoribbons. The band structures of these three types of PNRs as determined by PBE and HSE functional calculations are shown in Figures S9–S14. The corresponding band gaps and magnetic moments, also determined using the HSE and PBE functionals, are reported in Tables 3 and S4. The conduction-band minimum (CBM) and valence-band maximum (VBM) were set at the energies of the lowest unoccupied and highest occupied molecular orbitals, respectively, despite the inconsistency in the spin-up and spin-down parts.

Table 3. Band Gaps and Magnetic Moments of Pure and Edge-Terminated PNRs According to HSE Functional Computations

	zigzag		armchair		cliff	
edge termination	E_{gap}[a] (eV)	M (μ_B)	E_{gap}[a] (eV)	M (μ_B)	E_{gap}[a] (eV)	M (μ_B)
none	0.00 (Sm)	0.0083	0.94 (In)	0.0000	0.00 (Sm)	0.0000
HH	2.57 (In)	0.0062	1.64 (Di)	0.0000	1.65 (Di)	0.0000
HOH	2.54 (In)	0.0048	1.64 (Di)	0.0009	1.44 (Di)	0.0032
OHOH	2.50 (In)	0.0026	1.64 (Di)	0.0011	0.00 (Sm)	0.0164
OHO	2.34 (In)	1.9859	1.63 (Di)	2.0140	0.00 (Sm)	0.0230
OO	2.37 (In)	0.0863	1.81 (Di)	0.0094	1.82 (In)	0.0067
OH	2.35 (In)	1.9748	1.63 (Di)	1.9780	0.00 (Sm)	0.0050

[a]Sm, In, and Di denote semimetal, indirect, and direct, respectively.

The band gaps calculated using the HSE approach are commonly larger than those obtained using PBE, and they are close to the previous theoretical values.[58−60] The pure zigzag PNR shows semimetallic features, and all passivated zigzag PNRs are indirect-band-gap semiconductors. The band-gap values of the relatively stable configurations consisting of the OHOH-, OHO-, and OO-passivated zigzag PNRs are 2.50 eV (496 nm), 2.34 eV (530 nm), and 2.37 eV (523 nm), respectively, covering visible green regions. Their band gaps are larger than the thermodynamic water-splitting energy 1.23 eV, so they could be good photocatalysts. Moreover, the indirect-band-gap feature is favorable for the separation of electrons and holes in photocatalysis.

All of the armchair PNRs are semiconductors, and the band gaps are indirect for the pure structure and direct for the edge-passivated configurations. For the relatively stable OHOH- and OHO-terminated armchair PNRs, the (direct) band gaps are 1.64 eV (756 nm) and 1.63 eV (760 nm), respectively. Thus, these PNRs can be used as luminescent materials and applied in nanophotonic devices for thermal imaging and optical communications.[61] The pure and OHOH-, OHO-, OH-passivated cliff PNRs are metal-like, and the HH-, HOH-, and OO-terminated cliff PNRs show semiconducting behavior with direct and indirect gaps of 1.65 eV (752 nm), 1.44 eV (861 nm), and 1.82 eV (681 nm), respectively. Moreover, the pure and OHO-, OO-, and OH-passivated zigzag and armchair PNRs have some discrete levels, whereas the HH, HOH, and OHOH terminations cause no such levels, because the former groups contain unsaturated electrons whereas the latter do not. The OHO- and OH-passivated zigzag and armchair PNRs have large magnetic moments, whereas the pure and HH-, HOH-, OHOH-, and OO-passivated zigzag and armchair PNRs exhibit almost no magnetism. Furthermore, all of the passivated cliff PNRs have very small magnetic moments.

As far as we know, the PNR widths actually influence the electronic structure and formation energy. Quantum size effect becomes weaker when the ribbon width increases. The energy gaps of different edge-passivated zigzag and armchair nanoribbon change differently with the width.[27,60] For armchair PNRs, the band gaps change slightly when the PNR width exceeds 1 nm. Thus, the electronic properties of armchair PNRs are insensitive to widths up to 1 nm. For zigzag PNRs, the band gaps are obviously dependent on width. In general, the size dependence of properties weakens significantly[27] when the width is up to 1 nm. The width of the PRNs in this work was 1.36 nm, which was sufficient to allow the sensitivity of the formation energy to size to be neglected.

Figure 7 displays the density of states for OHOH- and OHO-passivated zigzag and armchair PNRs and for OHO- and OO-passivated cliff PNRs. These PNRs are semiconducting or

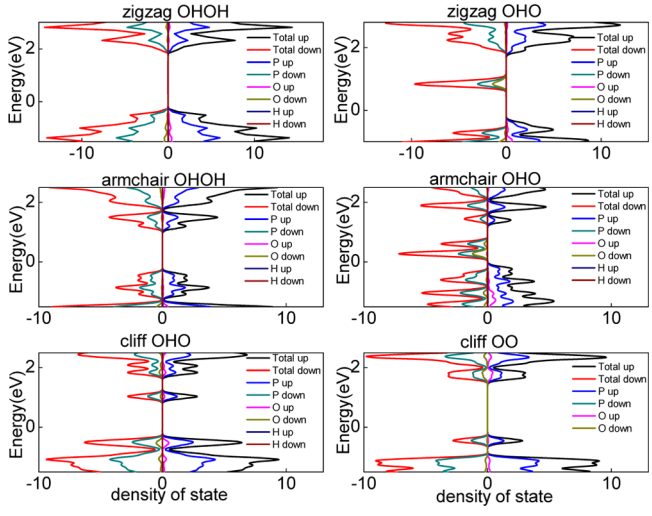

Figure 7. Total and partial densities of states for OHOH- and OHO-passivated zigzag PNRs, OHOH- and OO-passivated armchair PNRs, and OHO- and OO-passivated cliff PNRs having the lowest formation energies.

DOI: 10.1021/acs.jpcc.5b09159
J. Phys. Chem. C 2016, 120, 2149−2158

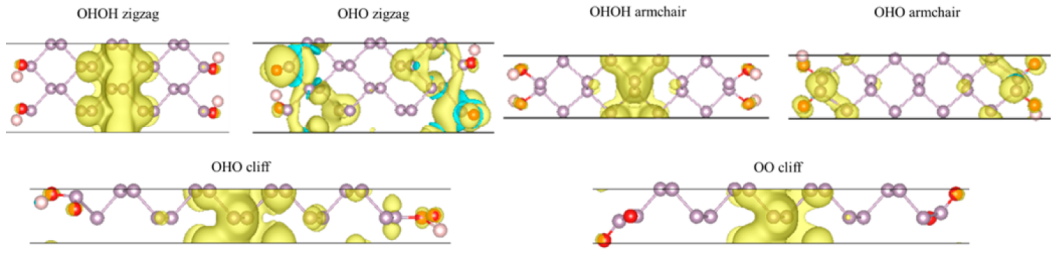

Figure 8. Spin-up (yellow) and spin-down (blue) densities for six types of configurations with the lowest formation energies in three types of PNRs.

semimetallic, with band gaps of 2.50 eV (indirect), 2.34 eV (indirect), 1.64 eV (direct), 1.63 eV (direct), 0.00 eV, and 1.82 eV (indirect). The CB and VB edges are mainly composed of P 3p orbitals with smaller quantities of O 2p orbitals. According to quantum theory, the emission intensity is proportional to electric dipole moment $q\vec{r}$. The VB and CB p orbitals are odd functions, and thus, electronsIc transitions between CB and VB states are forbidden. Therefore, the intrinsic photoluminescence in the visible and near-infrared ranges originates from intrinsic exciton and trion emissions.[62−64] By means of adjusting edges oxidization, the emission peaks can be tuned.

To explain the behavior of anisotropic adsorption, electronic density plots of the VBM and CBM are shown in Figure S15. The VBM and CBM of OHOH- and OHO-passivated zigzag PNRs are basically similar, mainly composed of delocalized and localized phosphorus 3p states. The edge P and passivation atoms make smaller contributions. In OHOH- and OHO-passivated armchair PNRs, the VBM and CBM electronic densities mainly originate from the internal P atoms, with a smaller contribution from the edge atoms, which is consistent with the density of states. The VBM of OHO-passivated cliff PNRs is similar to that of zigzag PNRs. It is interesting to note that the CBM of OHO-passivated cliff PNRs is composed of half of the P atoms in the nanoribbons. In OO-passivated cliff PNRs, the edge atoms make larger contributions to the VBM and CBM. Generally, the VBM is located at the top, middle, and bottom of the two sublayers, and the CBM is at the two subsurfaces.

Figure 8 shows the spin density distributions of these six PNRs. The isosurface values were taken as 2.6×10^{-5}, 5×10^{-4}, 2.5×10^{-5}, 3×10^{-5}, 1×10^{-4}, and 1.2×10^{-4} e/bohr^3 for the OHOH- and OHO-passivated zigzag PNRs, and OHOH- and OHO-passivated armchair PNRs, and OHO- and OO-passivated cliff PNRs, respectively. The OHOH-terminated zigzag and armchair PNRS and the OHO- and OO-terminated cliff PNRs mainly contain spin-up magnetic moments, although their values are small. The OHO-passivated zigzag and armchair PNRs contain spin-up and spin-down magnetic moments. The OHO- and OH-terminated zigzag and armchair PNRs have magnetic moments of approximately 2.00 μ_B (Figures 8 and S16), which are ascribed to unpaired electrons and reduced symmetry, similar to the two-dimensional group VI transition-metal dichalcogenides MX_2 (M = Mo, W; X = S, Se).[65] Therefore, by purposeful edge passivation, the magnetic properties of the PNRs can be tuned.

According to a previous report,[58] cell size can hardly influence magnetic moment. Thus, we used the same supercell size in calculating band structures and magnetic moments. A check for the possibility of preferential antiferromagnetic (AFM) coupling along the edge is important. Based on ref 58, AFM ordering in PNRs forms along the edge of pure zigzag PNRs. According to our calculations, OHO- and OH-passivated zigzag PNRs finally converge to AFM states, and the spin magnetic moments mainly originate from edge-atom states. Therefore, the final configurations are AFM configurations regardless of the initial FM or AFM configuration. For armchair PNRs, the conclusion is similar. For example, the ground states of OHO- and OH-passivated PNRs are AFM-state configurations (from Figures 8 and S16).

CONCLUSIONS

Edge passivation has a significant influence on the crystal and electronic structures of the three types of phosphorene nanoribbons (PNRs). Hydrogen atoms locate almost oppositely at the top and bottom edge P atoms in zigzag PNRs, whereas their adsorption behaviors closely rely on adjacent adsorbed impurities in armchair and cliff PNRs. The arrangements of oxygen atoms and hydroxyl groups depend on the ribbon-edge shapes and the nature of oxygen and hydroxyl groups themselves. For edge-passivated zigzag and armchair PNRs, the stable configurations are OHOH- and OHO-terminated ones, whereas the most stable cliff PNRs are OHO- and OO-terminated ones.

For stable PNRs, the VB and CB are mainly composed of phosphorus 3p orbitals, with small contributions from the passivation atoms. Pure zigzag nanoribbons are semimetallic, and the band gap is open after edge passivation. Edge saturation of armchair ribbons can enlarge the band gap. For cliff ribbons, pure and OHOH, OHO, and OH edge-passivated PNRs are semimetallic, whereas the HH-, HOH-, and OO-terminated structures are semiconducting. OHO and OH passivations give rise to large spin magnetic moments in zigzag and armchair ribbons, whereas all of the cliff ribbons exhibit small magnetic moments. Finally, the exciton or trion emissions are tunable within the visible and near-infrared regions through edge oxidization. Therefore, this study can direct future efforts to prepare PNRs with superior performance for photoelectronic and spinelectronic devices.

ASSOCIATED CONTENT

Supporting Information

The Supporting Information is available free of charge on the ACS Publications website at DOI: 10.1021/acs.jpcc.5b09159.

Figures showing original and optimized crystal structures, charge density distributions, two-dimensional Brillouin zone, band structures, CBM and VBM electronic densities, and spin densities and tables listing crystal structure parameters, band gaps, bond lengths, symmetry variation rules, energies of hydrogen and oxygen molecules, and magnetic moments (PDF)

DOI: 10.1021/acs.jpcc.5b09159
J. Phys. Chem. C 2016, 120, 2149−2158

AUTHOR INFORMATION

Corresponding Author

* E-mail: zjy@buaa.edu.cn. Phone: +86-10-82315351. Fax: +86-10-8231-7931.

Notes

The authors declare no competing financial interest.

ACKNOWLEDGMENTS

This project was financially supported by the National Science Foundation of China under Grants 91222110 and 51472013, the Specialized Research Fund for the Doctoral Program of Higher Education of China under Grant 20121102110027, and the State Key Laboratory of New Ceramic and Fine Processing at Tsinghua University (No. KF201414). The work was carried out at the National Supercomputer Center in Tianjin, China, and the calculations were performed on the TianHe-1A supercomputer. The VBM and CBM electronic density plots were drawn using the VASPMO program developed by Yang Wang, and the spin density plots were drawn using the VASPKIT program compiled by Dr. Wang and available at the website http://vaspkit.sourceforge.net/.

REFERENCES

(1) Bourdo, S.; Li, Z. R.; Biris, A. S.; Watanabe, F.; Viswanathan, T.; Pavel, I. Structural, Electrical, and Thermal Behavior of Graphite-Polyaniline Composites with Increased Crystallinity. *Adv. Funct. Mater.* **2008**, *18*, 432−440.

(2) Chhowalla, M.; Shin, H. S.; Eda, G.; Li, L. J.; Loh, K. P.; Zhang, H. The Chemistry of Two-dimensional Layered Transition Metal Dichalcogenide Nanosheets. *Nat. Chem.* **2013**, *5*, 263−275.

(3) Zhang, X. D.; Xie, X.; Wang, H.; Zhang, J. J.; Pan, B. C.; Xie, Y. Enhanced Photoresponsive Ultrathin Graphitic-Phase C_3N_4 Nanosheets for Bioimaging. *J. Am. Chem. Soc.* **2013**, *135*, 18−21.

(4) Dolui, K.; Pemmaraju, C. D.; Sanvito, S. Electric Field Effects on Armchair MoS_2 Nanoribbons. *ACS Nano* **2012**, *6*, 4823−4834.

(5) Zhang, S. L.; Yan, Z.; Li, Y. F.; Chen, Z. F.; Zeng, H. B. Atomically Thin Arsenene and Antimonene: Semimetal−Semiconductor and Indirect−Direct Band-Gap Transitions. *Angew. Chem., Int. Ed.* **2015**, *54*, 3112−3115.

(6) Zheng, H. X.; Duley, W. First-Principles Study of Edge Chemical Modifications in Graphene Nanodots. *Phys. Rev. B: Condens. Matter Mater. Phys.* **2008**, *78*, 045421.

(7) Wang, Y. Y.; Ni, Z. H.; Liu, L.; Liu, Y. H.; Cong, C. X.; Yu, T.; Wang, X. J.; Shen, D. Z.; Shen, Z. X. Stacking-Dependent Optical Conductivity of Bilayer Graphene. *ACS Nano* **2010**, *4*, 4074−4080.

(8) Li, L. L.; Wu, G. H.; Yang, G. H.; Peng, J.; Zhao, J. W.; Zhu, J. J. Focusing on Luminescent Graphene Quantum Dots: Current Status and Future Perspectives. *Nanoscale* **2013**, *5*, 4015−4039.

(9) Zhang, Y. B.; Tan, Y. W.; Stormer, H. L.; Kim, P. Experimental Observation of the Quantum Hall Effect and Berry's Phase in Graphene. *Nature* **2005**, *438*, 201−204.

(10) Li, L. K.; Yu, Y. J.; Ye, G. J.; Ge, Q. Q.; Ou, X. D.; Wu, H.; Feng, D. L.; Chen, X. H.; Zhang, Y. B. Black Phosphorus Field-Effect Transistors. *Nat. Nanotechnol.* **2014**, *9*, 372−377.

(11) Liang, L. B.; Wang, J.; Lin, W. Z.; Sumpter, B. G.; Meunier, V.; Pan, M. H. Electronic Bandgap and Edge Reconstruction in Phosphorene Materials. *Nano Lett.* **2014**, *14*, 6400−6406.

(12) Qiao, J. S.; Kong, X. H.; Hu, Z. X.; Yang, F.; Ji, W. High-Mobility Transport Anisotropy and Linear Dichroism in Few-Layer Black Phosphorus. *Nat. Commun.* **2014**, *5*, 4475.

(13) Wu, J. X.; Mao, N. N.; Xie, L. M.; Xu, H.; Zhang, J. Identifying the Crystalline Orientation of Black Phosphorus Using Angle-Resolved Polarized Raman Spectroscopy. *Angew. Chem.* **2015**, *127*, 2396−2399.

(14) Ling, X.; Liang, L. B.; Huang, S. X.; Puretzky, A. A.; Geohegan, D. B.; Sumpter, B. G.; Kong, J.; Meunier, V.; Dresselhaus, M. S. Low-Frequency Interlayer Breathing Modes in Few-Layer Black Phosphorus. *Nano Lett.* **2015**, *15*, 4080−4088.

(15) Dai, J.; Zeng, X. C. Bilayer Phosphorene: Effect of Stacking Order on Bandgap and Its Potential Applications in Thin-Film Solar Cells. *J. Phys. Chem. Lett.* **2014**, *5*, 1289−1293.

(16) Cai, Y. Q.; Zhang, G.; Zhang, Y. W. Layer-dependent Band Alignment and Work Function of Few-Layer Phosphorene. *Sci. Rep.* **2014**, *4*, 6677.

(17) Li, Y.; Yang, S. X.; Li, J. B. Modulation of the Electronic Properties of Ultrathin Black Phosphorus by Strain and Electrical Field. *J. Phys. Chem. C* **2014**, *118*, 23970−23976.

(18) Rudenko, A. N.; Katsnelson, M. I. Quasiparticle Band Structure and Tight-Binding Model for Single- and Bilayer Black Phosphorus. *Phys. Rev. B: Condens. Matter Mater. Phys.* **2014**, *89*, 201408.

(19) Li, W. F.; Yang, Y. M.; Zhang, G.; Zhang, Y. W. Ultrafast and Directional Diffusion of Lithium in Phosphorene for High-Performance Lithium-Ion Battery. *Nano Lett.* **2015**, *15*, 1691−1697.

(20) Padilha, J. E.; Fazzio, A.; da Silva, A. J. R. van der Waals Heterostructure of Phosphorene and Graphene: Tuning the Schottky Barrier and Doping by Electrostatic Gating. *Phys. Rev. Lett.* **2015**, *114*, 066803.

(21) Son, Y. W.; Cohen, M. L.; Louie, S. G. Half-Metallic Graphene Nanoribbons. *Nature* **2006**, *444*, 347−349.

(22) Hu, W.; Lin, L.; Yang, C. Edge Reconstruction in Armchair Phosphorene Nanoribbons Revealed by Discontinuous Galerkin Density Functional Theory. *Phys. Chem. Chem. Phys.* **2015**, *17*, 31397−31404.

(23) Zhang, X.; Xie, H. M.; Liu, Z. D.; Tan, C. L.; Luo, Z. M.; Li, H.; Lin, J. D.; Sun, L. Q.; Chen, W.; Xu, Z. C.; Xie, L. H.; Huang, W.; Zhang, H. Black Phosphorus Quantum Dots. *Angew. Chem.* **2015**, *127*, 3724−3728.

(24) Han, X. Y.; Morgan Stewart, H.; Shevlin, S. A.; Catlow, C. A. R.; Guo, Z. X. Strain and Orientation Modulated Bandgaps and Effective Masses of Phosphorene Nanoribbons. *Nano Lett.* **2014**, *14*, 4607−4614.

(25) Tran, V.; Yang, L. Scaling Laws for the Band Gap and Optical Response of Phosphorene Nanoribbons. *Phys. Rev. B: Condens. Matter Mater. Phys.* **2014**, *89*, 245407.

(26) Ramasubramaniam, A.; Muniz, A. R. Ab Initio Studies of Thermodynamic and Electronic Properties of Phosphorene Nanoribbons. *Phys. Rev. B: Condens. Matter Mater. Phys.* **2014**, *90*, 085424.

(27) Peng, X. H.; Copple, A.; Wei, Q. Edge Effects on the Electronic Properties of Phosphorene Nanoribbons. *J. Appl. Phys.* **2014**, *116*, 144301.

(28) Li, W. F.; Zhang, G.; Zhang, Y. W. Electronic Properties of Edge-Hydrogenated Phosphorene Nanoribbons: A First-Principles Study. *J. Phys. Chem. C* **2014**, *118*, 22368−22372.

(29) Ziletti, A.; Carvalho, A.; Campbell, D. K.; Coker, D. F.; Castro Neto, A. H. Oxygen Defects in Phosphorene. *Phys. Rev. Lett.* **2015**, *114*, 046801.

(30) Blochl, P. E. Projector Augmented Wave Method. *Phys. Rev. B: Condens. Matter Mater. Phys.* **1994**, *50*, 17953−17979.

(31) Kresse, G.; Hafner, J. Ab Initio Molecular Dynamics for Liquid Metals. *Phys. Rev. B: Condens. Matter Mater. Phys.* **1993**, *47*, 558−561.

(32) Jiang, J.-W.; Park, H. S. Negative Poisson's Ratio in Single-Layer Black Phosphorus. *Nat. Commun.* **2014**, *5*, 4727.

(33) Cai, Y. Q.; Ke, Q. Q.; Zhang, G.; Zhang, Y. W. Energetics, Charge Transfer, and Magnetism of Small Molecules Physisorbed on Phosphorene. *J. Phys. Chem. C* **2015**, *119*, 3102−3110.

(34) Momma, K.; Izumi, F. VESTA: a Three-Dimensional Visualization System for Electronic and Structural Analysis. *J. Appl. Crystallogr.* **2008**, *41*, 653−658.

(35) Guan, J.; Zhu, Z.; Tomanek, D. Phase Coexistence and Metal-Insulator Transition in Few-Layer Phosphorene: A Computational Study. *Phys. Rev. Lett.* **2014**, *113*, 046804.

(36) Wu, M. H.; Fu, H. H.; Zhou, L.; Yao, K. L.; Zeng, X. C. Nine New Phosphorene Polymorphs with Non-Honeycomb Structures: A Much Extended Family. *Nano Lett.* **2015**, *15*, 3557−3562.

DOI: 10.1021/acs.jpcc.5b09159
J. Phys. Chem. C 2016, 120, 2149−2158

(37) Brown, A.; Rundqvist, S. Refinement of the Crystal Structure of Black Phosphorus. *Acta Crystallogr.* **1965**, *19*, 684−685.
(38) Cai, C. Q.; Ke, Q. Q.; Zhang, G.; Feng, Y. P.; Shenoy, V. B.; Zhang, Y. W. Giant Phononic Anisotropy and Unusual Anharmonicity of Phosphorene: Interlayer Coupling and Strain Engineering. *Adv. Funct. Mater.* **2015**, *25*, 2230−2236.
(39) Wang, G. X.; Pandey, R.; Karna, S. P. Phosphorene Oxide: Stability and Electronic Properties of a Novel 2D Material. *Nanoscale* **2015**, *7*, 524−531.
(40) Ziletti, A.; Carvalho, A.; Trevisanutto, P. E.; Campbell, D. K.; Coker, D. F.; Castro Neto, A. H. Phosphorene Oxides: Bandgap Engineering of Phosphorene by Oxidation. *Phys. Rev. B: Condens. Matter Mater. Phys.* **2015**, *91*, 085407.
(41) Dai, J.; Zeng, X. C. Structure and Stability of Two Dimensional Phosphorene with =O or =NH Functionalization. *RSC Adv.* **2014**, *4*, 48017−48021.
(42) Tran, V.; Soklaski, R.; Liang, Y. F.; Yang, L. Layer-controlled Band Gap and Anisotropic Excitons in Few-layer Black Phosphorus. *Phys. Rev. B: Condens. Matter Mater. Phys.* **2014**, *89*, 235319.
(43) Liu, H.; Neal, A. T.; Zhu, Z.; Luo, Z.; Xu, X. F.; Tomanek, D.; Ye, P. D. Phosphorene: An Unexplored 2D Semiconductor with a High Hole Mobility. *ACS Nano* **2014**, *8*, 4033−4041.
(44) Maity, A.; Singh, A.; Sen, P. Peierls Transition and Edge Reconstruction in Phosphorene Nanoribbons. 2014, arXiv:1404.2469. arXiv.org e-Print archive. http://arxiv.org/abs/1404.2469 (Accessed Apr. 9, 2014).
(45) Island, J. O.; Steele, G. A.; Zant, H. S. J. D. Z.; Castellanos-Gomez, A. Environmental Instability of Few-layer Black Phosphorus. *2D Mater.* **2015**, *2*, 011002.
(46) Bechstedt, F. *Principles of Surface Physics*; Springer-Verlag GmbH: Berlin, 2003.
(47) Zhang, J.; Liu, H. J.; Cheng, L.; Wei, J.; Liang, J. H.; Fan, D. D.; Shi, J.; Tang, X. F.; Zhang, Q. J. Phosphorene Nanoribbon as a Promising Candidate for Thermoelectric Applications. *Sci. Rep.* **2014**, *4*, 6452.
(48) Carvalho, A.; Rodin, A. S.; Castro Neto, A. H. Phosphorene Nanoribbons. *Eur. Phys. Lett.* **2014**, *108*, 47005.
(49) Hod, O.; Barone, V.; Peralta, J. E.; Scuseria, G. E. Enhanced Half-Metallicity in Edge-Oxidized Zigzag Graphene Nanoribbons. *Nano Lett.* **2007**, *7*, 2295−2299.
(50) Fei, R. X.; Yang, L. Strain-Engineering the Anisotropic Electrical Conductance of Few- Layer Black Phosphorus. *Nano Lett.* **2014**, *14*, 2884−2889.
(51) Yu, S. H.; Conte, D. E.; Baek, S. H.; Lee, D. C.; Park, S. K.; Lee, K. J.; Piao, Y. Z.; Sung, Y. E.; Pinna, N. Structure-Properties Relationship in Iron Oxide-Reduced Graphene Oxide Nanostructures for Li-Ion Batteries. *Adv. Funct. Mater.* **2013**, *23*, 4293−4305.
(52) Kou, L. Z.; Frauenheim, T.; Chen, C. F. Phosphorene as a Superior Gas Sensor: Selective Adsorption and Distinct *I*−*V* Response. *J. Phys. Chem. Lett.* **2014**, *5*, 2675−2681.
(53) Avsar, A.; Vera-Marun, I. J.; Tan, J. Y.; Watanabe, K.; Taniguchi, T.; Castro Neto, A. H.; Ozyilmaz, B. Air-Stable Transport in Graphene-Contacted, Fully Encapsulated Ultrathin Black Phosphorus-Based Field-Effect Transistors. *ACS Nano* **2015**, *9*, 4138−4145.
(54) Gillgren, N.; Wickramaratne, D.; Shi, Y. M.; Espiritu, T.; Yang, J. W.; Hu, J.; Wei, J.; Liu, X.; Mao, Z. Q.; Watanabe, K.; Taniguchi, T.; Bockrath, M.; Barlas, Y.; Lake, R. K.; Ning Lau, C. Gate Tunable Quantum Oscillations in Air-stable and High Mobility Few-layer Phosphorene Heterostructures. *2D Mater.* **2015**, *2*, 011001.
(55) Kim, J.-S.; Liu, Y. N.; Zhu, W. N.; Kim, S.; Wu, D.; Tao, L.; Dodabalapur, A.; Lai, K. J.; Akinwande, D. Toward Air-Stable Multilayer Phosphorene Thin-Films and Transistors. *Sci. Rep.* **2015**, *5*, 8989.
(56) Wood, J. D.; Wells, S. A.; Jariwala, D.; Chen, K. S.; Cho, E. K.; Sangwan, V. K.; Liu, X. L.; Lauhon, L. J.; Marks, T. J.; Hersam, M. C. Effective Passivation of Exfoliated Black Phosphorus Transistors against Ambient Degradation. *Nano Lett.* **2014**, *14*, 6964−6970.
(57) Wan, B. S.; Yang, B. C.; Wang, Y.; Zhang, J. Y.; Zeng, Z. M.; Liu, Z. Y.; Wang, W. H. Enhanced Stability of Black Phosphorus Field-effect Transistors with SiO2 Passivation. *Nanotechnology* **2015**, *26*, 435702.
(58) Du, Y. P.; Liu, H. M.; Xu, B.; Sheng, L.; Yin, J.; Duan, C. G.; Wan, X. G. Unexpected Magnetic Semiconductor Behavior in Zigzag Phosphorene Nanoribbons Driven by Half-Filled One Dimensional Band. *Sci. Rep.* **2015**, *5*, 8921.
(59) Wu, Q. Y.; Shen, L.; Yang, M.; Cai, Y. Q.; Huang, Z. G.; Feng, Y. P. Electronic and Transport Properties of Phosphorene Nanoribbons. *Phys. Rev. B: Condens. Matter Mater. Phys.* **2015**, *92*, 035436.
(60) Guo, H. Y.; Lu, N.; Dai, J.; Wu, X. J.; Zeng, X. C. Phosphorene Nanoribbons, Phosphorus Nanotubes, and van der Waals Multilayers. *J. Phys. Chem. C* **2014**, *118*, 14051−14059.
(61) Ling, X.; Wang, H.; Huang, S. X.; Xia, F. N.; Dresselhaus, M. S. The Renaissance of Black Ohosphorus. *Proc. Natl. Acad. Sci. U. S. A.* **2015**, *112*, 4523−4530.
(62) Zhang, S.; Yang, J.; Xu, R. J.; Wang, F.; Li, W. F.; Ghufran, M.; Zhang, Y. W.; Yu, Z. F.; Zhang, G.; Qin, Q. H.; Lu, Y. R. Extraordinary Photoluminescence and Strong Temperature/Angle-Dependent Raman Responses in Few-Layer Phosphorene. *ACS Nano* **2014**, *8*, 9590−9596.
(63) Wang, X. M.; Jones, A. M.; Seyler, K. L.; Tran, V.; Jia, Y. C.; Zhao, H.; Wang, H.; Yang, L.; Xu, X. D.; Xia, F. N. Highly Anisotropic and Robust Excitons in Monolayer Black Phosphorus. *Nat. Nanotechnol.* **2015**, *10*, 517−521.
(64) Yang, J.; Xu, R. J.; Pei, J. J.; Myint, Y. W.; Wang, F.; Wang, Z.; Zhang, S.; Yu, Z. F.; Lu, Y. R. Optical Tuning of Exciton and Trion Emissions in Monolayer Phosphorene. *Light: Sci. Appl.* **2015**, *4*, e312.
(65) Zeng, H. L.; Cui, X. D. An Optical Spectroscopic Study on Two Dimensional Group-VI Transition Metal Dichalcogenides. *Chem. Soc. Rev.* **2015**, *44*, 2629−2642.

DOI: 10.1021/acs.jpcc.5b09159
J. Phys. Chem. C 2016, 120, 2149−2158